MDPI

Article

Collective Effects of Fire Intensity and Sloped Terrain on Wind-Driven Surface Fire and Its Impact on a Cubic Structure

Maryam Ghodrat [1,]*, **Ali Edalati-Nejad** [2] **and Albert Simeoni** [3]

1   School of Engineering and Information Technology, University of New South Wales Canberra, Canberra, ACT 2610, Australia
2   School of Science, University of New South Wales Canberra, Canberra, ACT 2610, Australia
3   Department of Fire Protection Engineering, Worcester Polytechnic Institute, Worcester, MA 01609, USA
*   Correspondence: m.ghodrat@unsw.edu.au

Abstract: The combined effects of percent slope and fire intensity of a wind driven line fire on an idealized building has been numerically investigated in this paper. The simulations were done using the large eddy simulation (LES) solver of an open source CFD toolbox called FireFOAM. A set of three fire intensity values representing different heat release rates of grassland fuels on different inclined fuel beds have been modeled to analyze the impact of factors, such as fuel and topography on wind-fire interaction of a built area. An idealized cubic structure representing a simplified building was considered downstream of the fire source. The numerical results have been verified with the aerodynamic measurements of a full-scale building model in the absence of fire effects. There is a fair consistency between the modeled findings and empirical outcomes with maximum error of 18%, which acknowledge the validity and precision of the proposed model. The results show that concurrent increase of fire intensity and terrain slope causes an expansion of the surface temperature of the building which is partially due to the increase of flame tilt angle upslope on the hilly terrains. In addition, increasing fire intensity leads to an increase in the flow velocity, which is associated with the low-pressure area observed behind the fire front. Despite limitations of the experimental results in the area of wind-fire interaction the result of the present work is an attempt to shed light on this very important problem of fire behavior prediction. This article is a primary report on this subject in CFD modeling of the collective effects of fire intensity and sloped terrain on wind driven wildfire and its interaction on buildings.

Keywords: wildfire; LES; terrain slope; fire intensity; FireFOAM

1. Introduction

Wind and topography, including terrain slope, together with the vegetation (fuel type), are commonly accepted to be the dominant factors affecting wildfires dynamic [1].

Wildfires usually occur in complex topography which impacts the spread of the flame in various ways. Wind makes the scenario even more complex with the combined interaction of slope and intensity of the fire front and in many cases; this is the situation fire management authorities and firefighters may need to face [2].

It is commonly known that fire speeds up uphill, and numerous disastrous incidents of fire fighter fatalities have been reported in hilly terrains [3]. Many researchers [4–6] proposed semi-empirical or empirical fire models for fire behavior prediction systems and estimate the impact of sloped terrain using a spreading factor. A correlation between slope and wind was developed by Sharples [7], which indicates the slope and wind effects have the same trigger. That is to say, with the increase of wind speed or slope angle, the angle between the flame and unburnt fuel bed decreases, and the heat transfer increases accordingly. In another research, Dupuy and Maréchal [8] found out that radiation heat transfer from the unburnt area to the unburned fuel bed is dominant once the slope angle

increases from 0° to 20° however by increasing the slope angle to 30° the convection becomes dominant.

Experiments conducted on the slope fire without the presence of wind are required to identify the slope effect. Van Wagner [9] conducted a series of laboratory experiments on the influence of upslope on fire dynamics and Rothermel [5] assessed the impact of sloped terrain on fire propagation by running laboratory upslope fires in no-wind environments. Viegas [10] proposed a line fire rotation assumption to analyze the impact of slope and to explain the change of fire shape. By conducting a number of laboratory tests, Dupuy [11] noted that particular fuel bed sizes were too small for investigating slope effects. Other researchers, such as Weise and Biging [12] and Mendes-Lopes et al. [13], investigated the collective impacts of wind and slope in laboratory conditions and reported some valuable data on slope fires spreading in no-wind environments. Vega et al. [14] and Fernandes et al. [15] developed empirical models based on a series of field experiments on fire spread over a sloping terrain smaller than 20 degrees which were similar to the McArthur model [6]. All the above-mentioned experiments used small fuel beds with fixed fire intensity and no attempt was made to examine the impact of fuel bed load associated with different fire intensities on fire wind interaction and particularly not been done on Wildland Urban Interface (WUI). Most of the available studies are on the effect of slope on the rate of spread of the fire. One such study is an experimental investigation done by Cheney et al. [16] on several field tests. They measured the impact of fire width on the rate of spread with wind on the flat terrain. The increase in the rate of spread with increasing slope angle was observed by Dupuy [17]. Edalati-nejad et al. [18] conducted a numerical study on the effect of sloped terrain on a line fire and its influence on a structure. The authors performed a time-dependent numerical study to investigate how a line fire affects a cubic obstacle placed on a sloped landscape. In their study, a sloped field with various angles of 0 to 30° under a range of wind velocities was simulated. Fire intensity was considered a constant value. Their results showed that under a single fire intensity value, raising the upslope terrain angle causes temperature growth near the structure. A numerical investigation on the impact of terrain slope on wind enhancement by a point source fire was carried out by Eftekharian et al. [19]. In the study, the impact of terrain slope on downstream wind flow as well as the location at which local maximum wind enhancement occurs was investigated. Results indicated that by an increase in terrain upslope angle, wind enhancement intensifies considerably. In their study, the impact of fire intensity on the downstream flow presence of the building was not investigated.

In addition to the terrain slope, fire intensity associated with the fuel load, type, and moisture of the fuel plays a crucial role in the fire dynamic modeling. In fact, intensity is one of the main characteristics of any fire regime [20,21]. Basically, in the context of fire science, fire intensity defines the physical concept of combustion development of energy discharge from the fuel bed, such as bush or grassland, forest, or any other type of material that can be considered as fuel for the fire. Therefore, the expression 'intensity' is described as a gauge of the time-averaged energy flow or the energy per unit volume multiplied by the velocity where energy is transferring. The unit of the resultant vector is W m^{-2} [22].

Rothermel [5] introduced a term called reaction intensity in his fire propagation model. This term represents the heat source and is consistent with the definition given by Jon E. Keeley [23]. However, there is a need for a much more thorough use of the term "intensity". One alternative can be fire-line intensity, which is defined as the rate of heat transfer per unit length of the fire line (kW m^{-1}) [24]. Fireline intensity signifies the radiative or convective energy in the flame front and is a significant characteristic for fire spread; therefore, fire intensity holds important information for fire suppression activities and has been incorporated into rating calculations of fire danger [25–27]. In the literature, the measure that represents fire intensity is fire-line intensity [28,29], which is misleading as much fire research measures, such as energy release from fire, provide a more practical system of measurement.

The concept of fire intensity is most regularly used in forest fires or grassland fires [30]. Many studies in the literature indicate that there is a relationship between the intensity of the fire line and flame length and the blazing height of coniferous tree crowns [31–34]. However, some fire consequences are more tightly linked to various fire intensity measures. Quantifying these other measures is usually necessary because fire-line intensity may be feebly associated with extreme temperature or heating duration [33,35].

Fire-line intensity offers information for more effective management of fire, temperature, and heating duration (residence time). Additionally, it can provide more important information for fire management activities, such as prescribed burning that requires maintaining vulnerable ecosystem elements. Other metrics, such as radiative energy, are more easily quantifiable for fire intensity in remote imaging analyses of fire impacts [36,37].

In addition, recently structure loss in wildland fires has substantially grown, which is mainly impacted by extended development in countryside areas, variations in fuel management strategies, and extreme weather due to climate change all of which are expected to upsurge in the future [38]. Furthermore, changing the area around a structure—particularly the adjacent fuel and landscape will influence the coverage conditions that affect the structure [39]. Therefore, understanding the flow field and heat transfer around and on the structures and mitigation tactics to reduce them is one method of decreasing WUI losses. Detailed information on structure burning in forced flow (strong wind) will also be important to enhancing risk-based forecasting tools and the development of potential WUI fire simulations [40].

Robust knowledge of the fundamental procedures that handle wildland fires is essential for delivering science-based explanations to the challenges wildfire pose to the ecosystem and society. A Computational Fluid Dynamics (CFD) simulation of wildland fire provides a significant path for enhancing this knowledge. Findings that are provided using CFD platforms have demonstrated potential in offering new understandings into a range of subjects linked to the wildland fires dynamics or at the very least have underlined areas that need sustained scientific research. For instance, the significance of fuel composition within a variety of sizes [40–42], the significance of flame configuration [43,44], and many more [45–52].

As these models evolve, it is crucial to make sure that they are implemented appropriately and tested rigorously against relevant experimental data [53,54]. To make the prediction of the complicated behavior of wildfires more feasible, various influencing factors have usually been treated independently. Many known studies have investigated wind, slope, or fire intensity effects separately. To the best of our knowledge, only relatively simple cases in which slope gradients are varied under constant fuel load (fire intensity) are studied in the literature [55–59]. Some other studies are available on the effect of wind velocities and slopes in which the spread rate is associated with the wind velocity or local terrain slope [60–64]. A survey in the literature reveals that despite its great significance the combined influence of terrain slope and fuel load on wind-driven surface fire has not yet been studied.

The key objective of this research is to develop a quantifiable and methodical assessment of the causes triggering the variation of the velocity profile and surface temperature of a structure located on different uphill terrains with fire sources of various intensities. This research is an early effort to model a wind-driven fire-line interaction with an idealized building. The influence of changing fire intensity values on an idealized building located on different uphill terrains has been simulated using FireFOAM CFD solver [65]. FireFOAM is employed to measure the thermal updraft loads on the building subjected to a bushfire (with varying intensities) that is infringing on the wildland-urban interface. Fire dynamic behavior is also examined and observations on the flame structure under different fire-line intensities are discussed. The present study aims to offer useful information related to the effect of the intensity of line fires on building ignition, enhancement of wind by fire, and strong winds/pressure gradients that can influence the structures' integrity and the

damage that could cause. It is notable to mention that the impact of strong fire-enhanced winds is largely neglected as part of the current risk managing code (with APZs, etc.).

2. Model Description

The computational domain in this study involves a rectangular field with a dimension of $50 \times 30 \times 25$ m as demonstrated in Figure 1a. A cubic structure representing an idealized building with a size of 6 m in all directions, is located 25 m on the fire downstream. The fire source is a line fire running across the entire domain and placed 20 m upstream of the building to resemble a line fire pattern [66].
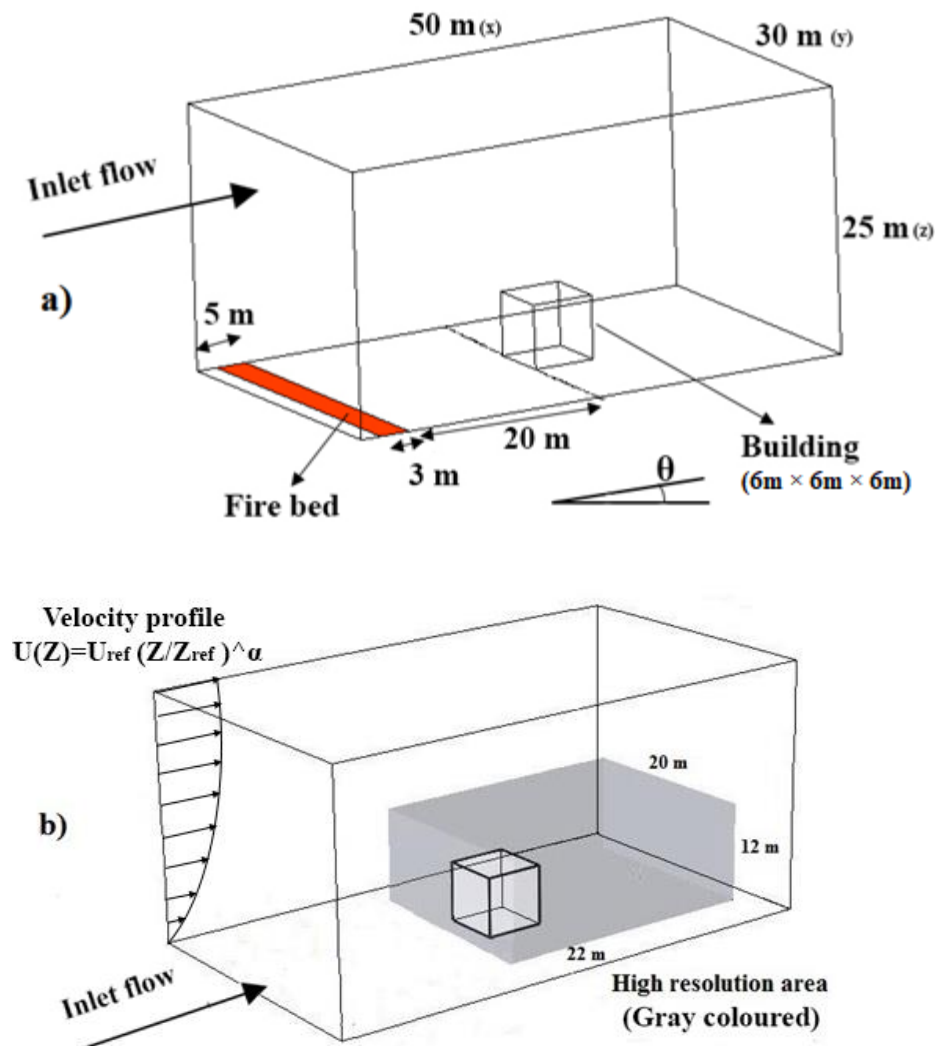

Figure 1. Schematic of computational domain and the location of the building (**a**) total domain; (**b**) subdomain geometry (location of the refinement zone).

The size of the building is identical to the size of Silsoe building in the experimental study of Richards and Hoxey [67] (6 m $\times$ 6 m $\times$ 6 m), which was done on flat terrain and provides a series of essential scale data on the underlying aerodynamics of low-rise buildings under different wind loads. In this study, agreeing to the suggestions given by Richards and Norris [68], the borders of the field are sufficiently far off the structure to prevent the adverse impacts of boundary conditions.

To examine the collective effects of fire intensity and upslope terrain on the cubic structure downstream of the fire, a 3 m width fire bed flaming through the whole domain was placed 20 m upstream of the structure. Fuel has been chosen to ne methane with combustion heat of 45,435 kj/kg [43] to give intensity [24] of 10, 14, and 18 MW/m. These

intensities are comparable to a conventional bushfire with rate of spread of 0.75–0.8 m/s and a load of fuel equal to 0.4–0.6 kg/m^2 in common grassland according to [69].

To investigate the collective impacts of fire intensity and sloped terrain in this research, the angle of attack of the domain is set at four distinct upslope angles equal to $\theta = 0°$, 10°, 20°, and 30°. The horizontal slope namely the domain attack angle, θ, is defined as the gravitational acceleration angle with the z axis of the simulation field, which is specified as two non-zero factors:

$$gx = -g \, \sin{(\theta)} \text{ and } gz = -g \, \cos{(\theta)}, \tag{1}$$

For the initial internal field, inlet, outlet, and top boundaries, the atmospheric pressure is applied. Free slip (zero gradient) boundary condition is considered for the side and top boundaries. The no-slip wall is used in the ground and building surfaces to have the near-wall treatment of turbulent flow. Using self-adapting wall function provides a higher resolution closer-to-wall eddy flows for a finer wall mesh comparable to the dimensionless wall distance parameter of values lower than 5 (y+ < 5 m). This implies that the turbulent boundary layer is fully solved up to the viscous sublayer. The initial temperature of the domain is 300 K, and the initial velocity follows the power-law velocity profile given in Equation (2). To generate more realistic inflow data and to be able to consider for turbulent inflow conditions, the boundary layer at the ambience is implemented using a power-law velocity profile (Equation (2)). This is a simple and yet efficient technique to lay over random oscillations on average velocity outline and to reduce the cost allied with causing the inflow data [70]. Therefore, in this study the random noise with the mean flow velocity is implemented at the domain inlet to rebuild the turbulent flow fluctuations. The power-law velocity profile used at the domain inlet is given in Equation (2) and also shown in Figure 1b.

$$U(Z) = U_{ref} \left(\frac{Z}{Z_{ref}} \right)^{\alpha}, \tag{2}$$

where Z_{ref} is the reference altitude identical to the building's height (6 m), and U_{ref} is the reference velocity that is chosen as 6 m/s in this study. α is stipulated based on the terrain category in the experimental investigation of [71] and selected as 0.16. The primary temperature and velocity of the field are chosen as 300 K and 0 m/s, respectively.

To generate more precise computational results, close to the cube (representing the idealized building) and downstream of the fire, close to-wall regions with dimension of $22 \times 20 \times 12$ m is created as a subfield with higher-resolution grid (See Figure 1b).

3. Numerical Method

Numerical simulations were performed using FireFOAM [65], which is an open-source software package composed of physical models related to heat transfer, combustion, and turbulent diffusion flames. FireFOAM is a large eddy simulation (LES)-based solver of OpenFOAM that is a C++ toolbox for developing customized numerical codes [72]. The privilege of FireFOAM is that the solver integrates several methodical CFD sub models account for range of processes happen in fire dynamic. It has been effectively employed in a number of practical purposes including pyrolysis of the solid fuels [73], fire suppression [74] and fire-wall interaction [75]. FireFOAM has also been shown to be an efficient means in wildfire simulations [76].

The Favre-filtered continuity, momentum, energy, species, and state equations for fully compressible flow is solved, which is the most common form representing fire dynamics [77]:

$$\frac{\partial \overline{\rho}}{\partial t} + \frac{\partial (\overline{\rho} \widetilde{u}_i)}{\partial x_i} = 0 \tag{3}$$

$$\frac{\partial (\overline{\rho} \widetilde{u}_i)}{\partial t} + \frac{\partial (\overline{\rho} \widetilde{u}_i \widetilde{u}_j)}{\partial x_i} = \frac{\partial}{\partial x_j} \left[\overline{\rho}(\upsilon + \upsilon_t) \left(\frac{\partial (\widetilde{u}_i)}{\partial x_j} + \frac{\partial (\widetilde{u}_j)}{\partial x_i} - \frac{2}{3} \frac{\partial (\widetilde{u}_k)}{\partial x_k} \delta_{ij} \right) \right] - \frac{\partial (\overline{P})}{\partial x_i} + \overline{\rho} g_i, \tag{4}$$

$$\frac{\partial\left(\overline{\rho}\widetilde{h}\right)}{\partial t} + \frac{\partial\left(\overline{\rho}\widetilde{u}_j\widetilde{h}\right)}{\partial x_j} = \frac{D\overline{P}}{Dt} + \frac{\partial}{\partial x_j}\left[\overline{\rho}\left(\alpha_t + \frac{v_t}{Pr_t}\right)\left(\frac{\partial\widetilde{h}}{\partial x_j}\right)\right] + \dot{q}''' - \nabla.\dot{q}_r'', \tag{5}$$

$$\frac{\partial\left(\overline{\rho}\widetilde{Y_m}\right)}{\partial t} + \frac{\partial\left(\overline{\rho}\widetilde{u}_j\widetilde{Y_m}\right)}{\partial x_j} = \frac{\partial}{\partial x_j}\left[\overline{\rho}\left(D_c + \frac{v_t}{Sc_t}\right)\frac{\partial\left(\widetilde{Y_m}\right)}{\partial x_j}\right] + \omega_m, \tag{6}$$

$$\overline{P} = \overline{\rho}R\widetilde{T}, \tag{7}$$

where "$^{-}$" and "$\sim$" indicates spatial and Favre filtering, correspondingly. p is the static pressure, h signifies the total enthalpy, Y_m is the mass fraction of species m, g is the gravitational acceleration. Pr_t, Sc_t, D_c, v, v_t, P, R, α_t, δ and ω_m are the turbulent Prandtl number, turbulent Schmidt number, laminar diffusion coefficient, laminar viscosity, turbulent viscosity, density, gas constant, thermal diffusion coefficient, Kronecker delta and production/sink rate of species m due to gas reaction, respectively. Coupled velocity and pressure is applied in the PIMPLE scheme, which is used by FireFOAM, and the combustion Eddy Dissipation Model (EDM) is also employed in this numerical model. The model was initially proposed by Magnussen et al. [78,79]. In this model, turbulent mixing and combustion take place in finer structures (or smaller dissipative eddies) close to the Kolmogonov scale [80]. In this study, the turbulence model of the Large Eddy Simulation (LES) is applied. The model is more accurate than RANS models. In this model, the convolution between the spatial field and the filter function defines the spatial filtering operation [81]. The turbulent intensity is calculated at approximately 11% at the inlet top height. This makes an approximately 5% turbulent intensity at the building height location.

4. Model Validation

To validate the numerical model, two sets of experimental data are used. The first experimentation is associated with the measurement of pressure along the centerlines (vertical and horizontal) of the Silsoe 6 m cube proposed by Richards and Hoxey [67]. In the research done by [67], a complete set of data is prepared in a non-intersecting data block of the cube surface tap pressure along with the source upstream approach flow measured at the cube height.

As a whole scale cube test was done in the wind condition given by nature, each data block was distinct regarding the average conditions and there is no chance to precisely duplicate an experiment several times, as may possibly be conducted in a wind tunnel. Consequently, Richards and Hoxey [67] were able to manage the data in a way that a large number of blocks recorded were generated where the pressure coefficients were calculated by normalizing with the wind dynamic pressure at a reference position.

The second experiment applied to validate the current simulation is the investigation of Castro and Robins [82]. They investigated the flow over surface-mounted cubes in uniform, irrotational, and sheared, turbulent flows where measurements of body surface pressures and average and oscillating velocities within the wake were reported.

In conjunction with the two mentioned empirical analyses which were conducted in no-fire conditions, the present numerical model is also validated with the numerical work of He et al. [83]. He et al. [83] used Fire Dynamic Simulation (FDS) package to predict the distribution of pressure coefficient over a building under no-fire conditions.

Because the Eddy Dissipation Concept (EDC) is primarily controlled by turbulent mixing, fire dynamic behavior is closely associated with the aerodynamics of the building. Therefore, the pressure distribution on the structure in a no fire condition is a sensible measure that indicates the accuracy and validity of the numerical findings.

A grid sensitivity analysis is carried out to minimize the numerical uncertainties. With that, three sets of different grid sizes are created into the domain including 4,600,000, 7,800,000, and 9,500,000 structure grids. The subdomain grid resolution is five times greater than the primary field in which a three grid sets of ($176 \times 160 \times 96$, $210 \times 191 \times 114$, and $224 \times 204 \times 122$) were examined. The outcomes of the mesh sensitivity analysis suggested

that growing the number of the cells primarily increases the mean pressure coefficient but further increase slightly affects the pressure profile. Therefore, the grid size of 7,800,000 was used for the simulations. All modeling was done for an overall time of 20 s after injecting of the fuel. It should be noted that a 20 s initial run is conducted to obtain quasi-fully developed turbulence prior to the initiation of the fire.

The simulation results of the average coefficient of pressure alongside the centerlines over the front surface of the building, at the top and rear sides of the cubic building (demonstrated by 0–1–2–3 solid lines) are mapped and shown in Figure 2.
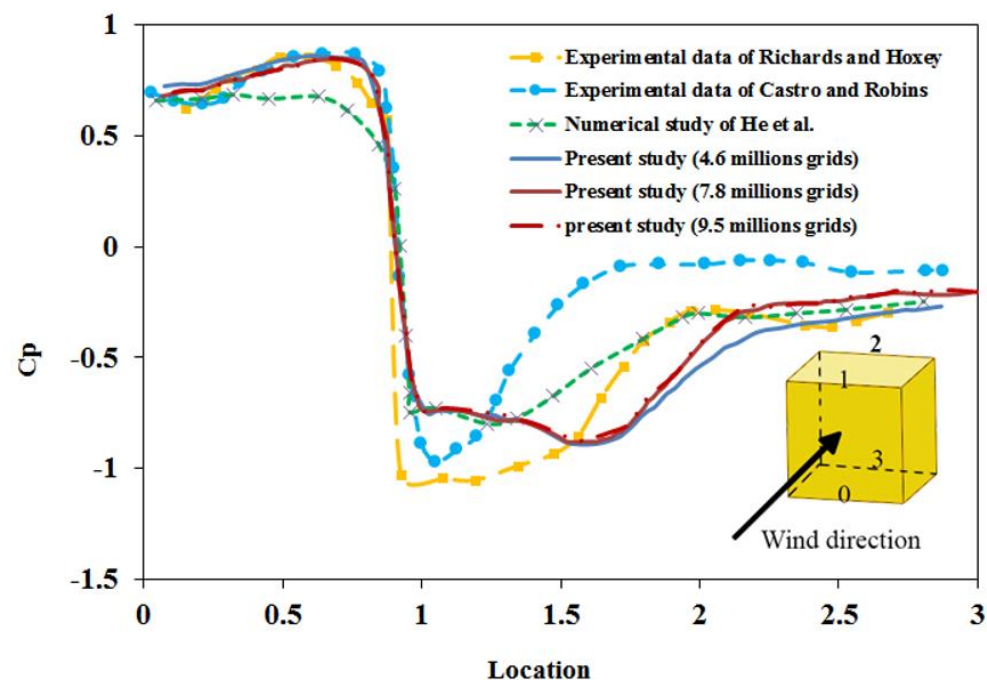

Figure 2. Comparison of the mean pressure coefficient for the experimental studies of [64,74], numerical simulation of [75], and three different grids number for the presented study.

The numerical results are compared with the experimental outcomes of Richards and Hoxey [67] and Castro and Robins [82] and the numerical results of He et al. [34]. Validation results are shown in the author's previous study [18], which suggested that even though there is an acceptable consistency between the experimental and numerical data on the windward and leeward faces (0–1 and 2–3 lines), perceptible inconsistencies still exist across the roof face of the cube (1–2 line). These discrepancies which were also noted in other investigations included in Figure 2, can be associated with the great scatter of wind velocity data and direction data. This matter significantly affects the separation zones in the corners and the pressure distribution across the roof of the idealized building. Moreover, as the variations of wind pressure on the building are mainly because of the large-scale changes, the dimension of the modeling field can restrict the size of the biggest eddy and impact the outcome in an unsatisfactory way. The highest error of 18% is observed in location 1.25.

5. Result and Discussion

This study investigates the simulated impact of a dynamically variable wind field on a fixed heat source, delineating a WUI fire configuration. The simulations allowed for analysis of the transient fire performance that could be anticipated. The key aim of this work, therefore, is to create a validated, CFD code to simulate the collective impacts of wind-driven fire intensity and slope terrain in a WUI fire pattern. From both modeling and experimental points of view, the intensity of the fire and topography including sloped terrain are key features in assessing wildfire impacts on structures in WUI.

Figure 3 depicts the pattern of the flow for the change in velocity in the fire domain, in the stabilized state of the fire. The contour of vertical transects of stabilized streamwise velocity component (Ux = velocity component in the X direction) and corresponding velocity vectors in the flat terrain and 3 other sloped terrains (θ = 10°, 20°, and 30°) for various fire intensities of 10, 14, and 18 MW/m in a constant crosswind reference velocity of 6 m/s is presented.
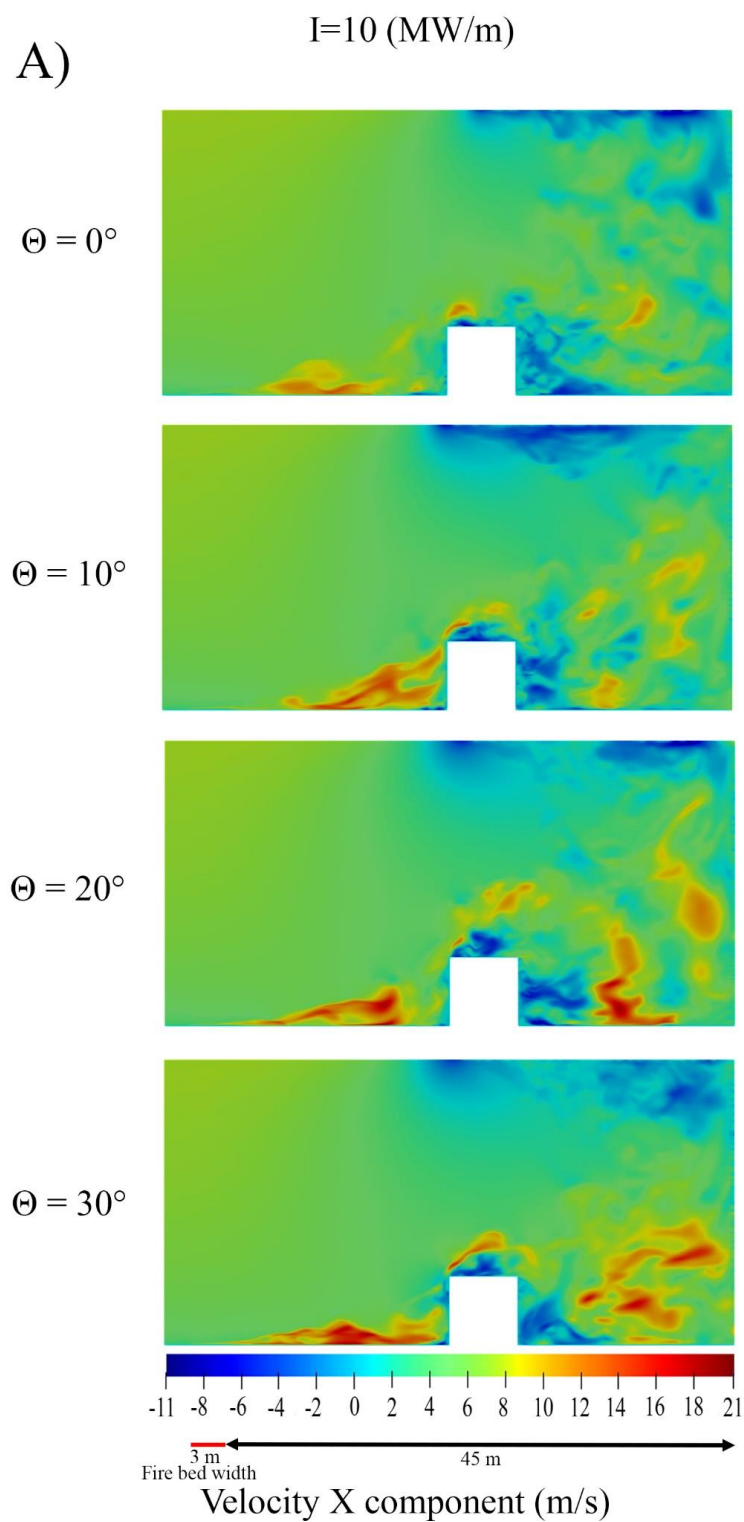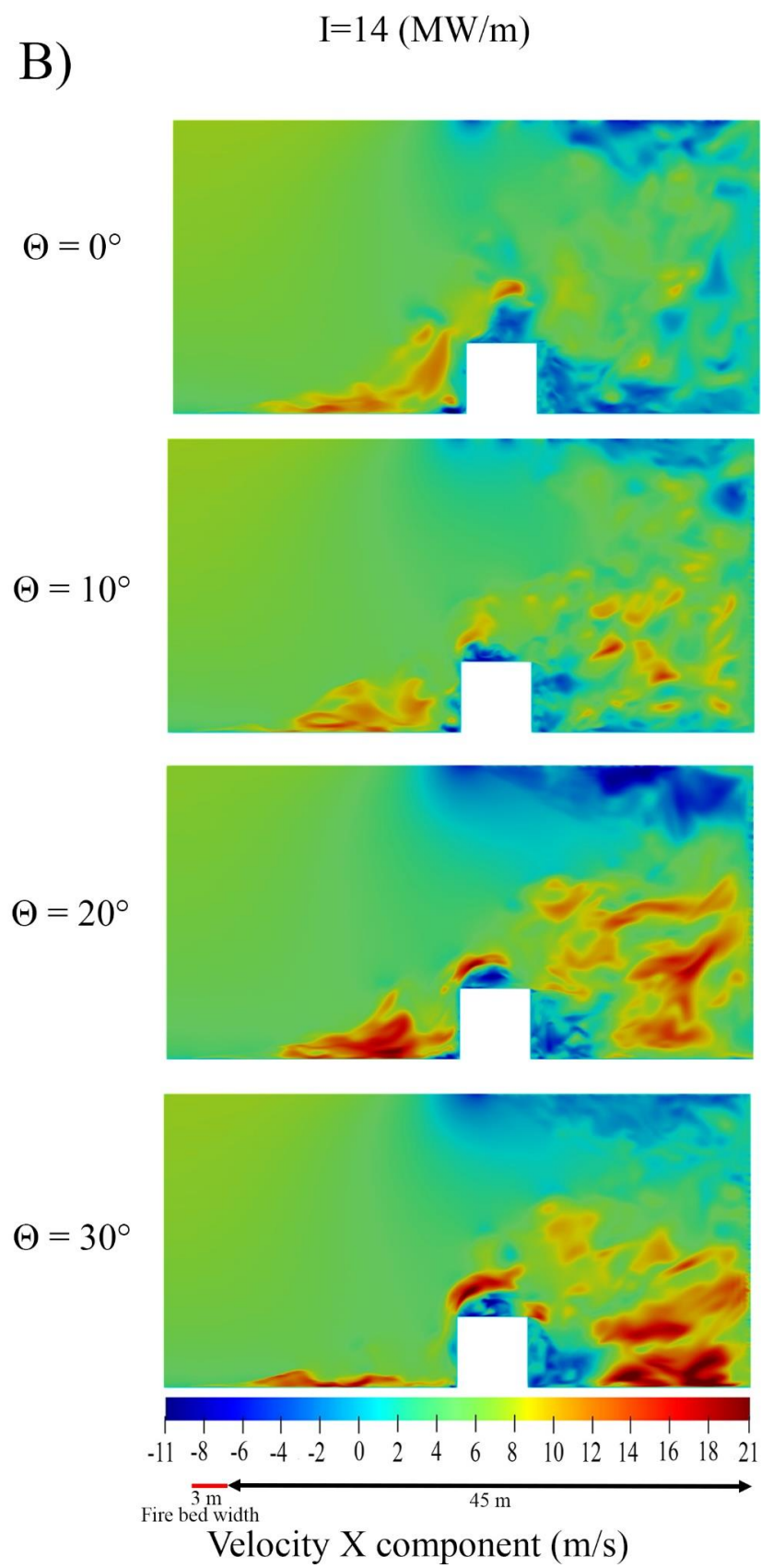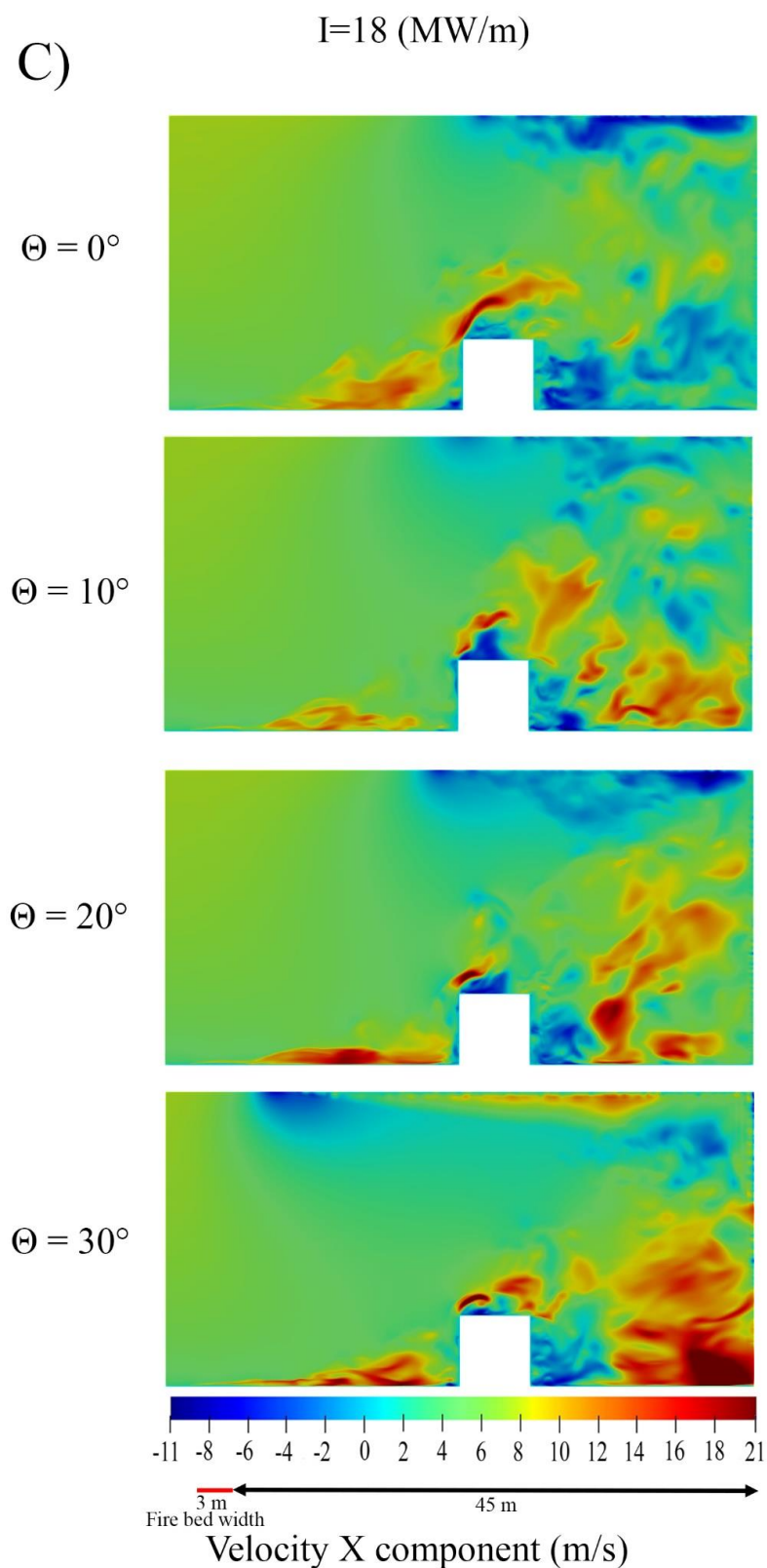

Figure 3. *Cont.*

Figure 3. *Cont*.

Figure 3. Vertical transects of the stabilized state streamwise velocity component (Ux) for the reference velocity U_{ref} = 6 m/s in various fire intensities and slopped terrains (**A**) Fire intensity of 10 (I = 10 MW/m), (**B**) Fire intensity of 14 (I = 14 MW/m) and (**C**) Fire intensity of 18 (I = 18 MW/m).

As can be seen in this figure, the simulated fire plum is tilted towards the ground downstream of the fire bed. This is primarily because inertia forces are prevalent in this

region. Furthermore, air entrainment hooked on the turbulent surface fire generates a low-pressure zone in the fire-ground attachment area ahead of the fire. As a result, the fire plume is expedited and creates a strong stream shape in a comparatively small area nearly connected to the floor instantly downwind of the fire source.

Comparing Figure 3A with Figure 3B,C for each terrain slope (flat terrain and θ = 10°, 20° or 30°), it is evident that by rising fire intensity from I = 10 MW/m to I = 14 MW/m and I = 18 MW/m, hot air plume around the flame zone moves forward in a faster pace. This is due to having a low-pressure zone ahead of the fire source because of the heated air in that area. This would form a low-density air region that generates an extra stream behind the fire plume and increases the air velocity downstream of the fire source.

On the other hand, for each fire intensity (I = 10 MW/m to I = 14 MW/m or I = 18 MW/m), increasing the terrain slope (upslope terrain) strengthens the Coanda effects [84] and triggers the flow to be more tilted and to stay connected to the ground instantly downstream of the fire. This is because of the creation of a component of buoyancy force in the wind direction [19]. The Coanda effect is defined as when a jet flow attaches itself to a nearby surface and remains attached due to inhibited entrainment of ambient fluid near the solid [84]. As shown in Figure 3, the collective effect of fire intensity and terrain slope will lead to the creation of a non-uniform region with random movements of the fire plume downstream of the fire source, which is associated with the unbalance buoyancy force and inertial flow from upstream toward downstream of the domain.

As shown, by increasing the sloping terrain for each fire intensity, the fire-ground bond area is stretched due to the oscillating behavior of the fire plume downstream of the fire. In addition, a recirculation area is observed downstream of the fire, behind the building which is associated with the reverse flow. In fact, having a pressure drop and wake along with a buoyant instability [85] results in the formation of a higher temperature air region behind the building. This phenomenon intensifies, with the growth of terrain slope, which is directly linked to the increase of buoyant flow instability which is happening due to changes in buoyancy force direction. The simulation results show that the maximum magnitude of flow disturbance occurs in the highest upslope angle and fire intensity (I = 18 MW/m and θ = 30°). At this Downstream of the fire, at the back of the building, a recirculation region because of reverse flow can be seen. This mostly happened due to pressure cut out and wakes together with a buoyant instability [85], which results in the creation of hot air zone at the back of the building. The mentioned incident escalated with a combined increment of fire intensity and slope terrain because of shifting in buoyancy force direction.

In addition, the presence of a building can substantially contribute to changing the plume attachment length. In other words, with increasing fire intensity and terrain slope the building generates premature buoyant fluxes, and the fire plume lift-off distance reduces in front of the structure.

Figure 4 shows the collective impacts of three different fire intensities and sloped terrain on the temperature distribution around the building at a constant crosswind velocity of U_{ref} = 6 m/s. The contours are demonstrated in the stabilized state of the fire. As shown, at each sloped terrain (flat terrain, θ = 10°, 20° or 30°), increasing the intensity of the fire causes an increase in the temperature profile downstream and near the building. Results also show that the greater the intensities at steeper slopes change the downstream temperature considerably, in that the space behind the building experiences noticeably higher temperature variation of up to 1500 K at the highest fire intensity and steepest sloped terrain considered in this study (I = 18 MW/m and θ = 30°). The reason for temperature enhancement at the space behind the building with an increase in the terrain slope is due to increase in the tilt angle of the flame and the high temperature plume recirculation.
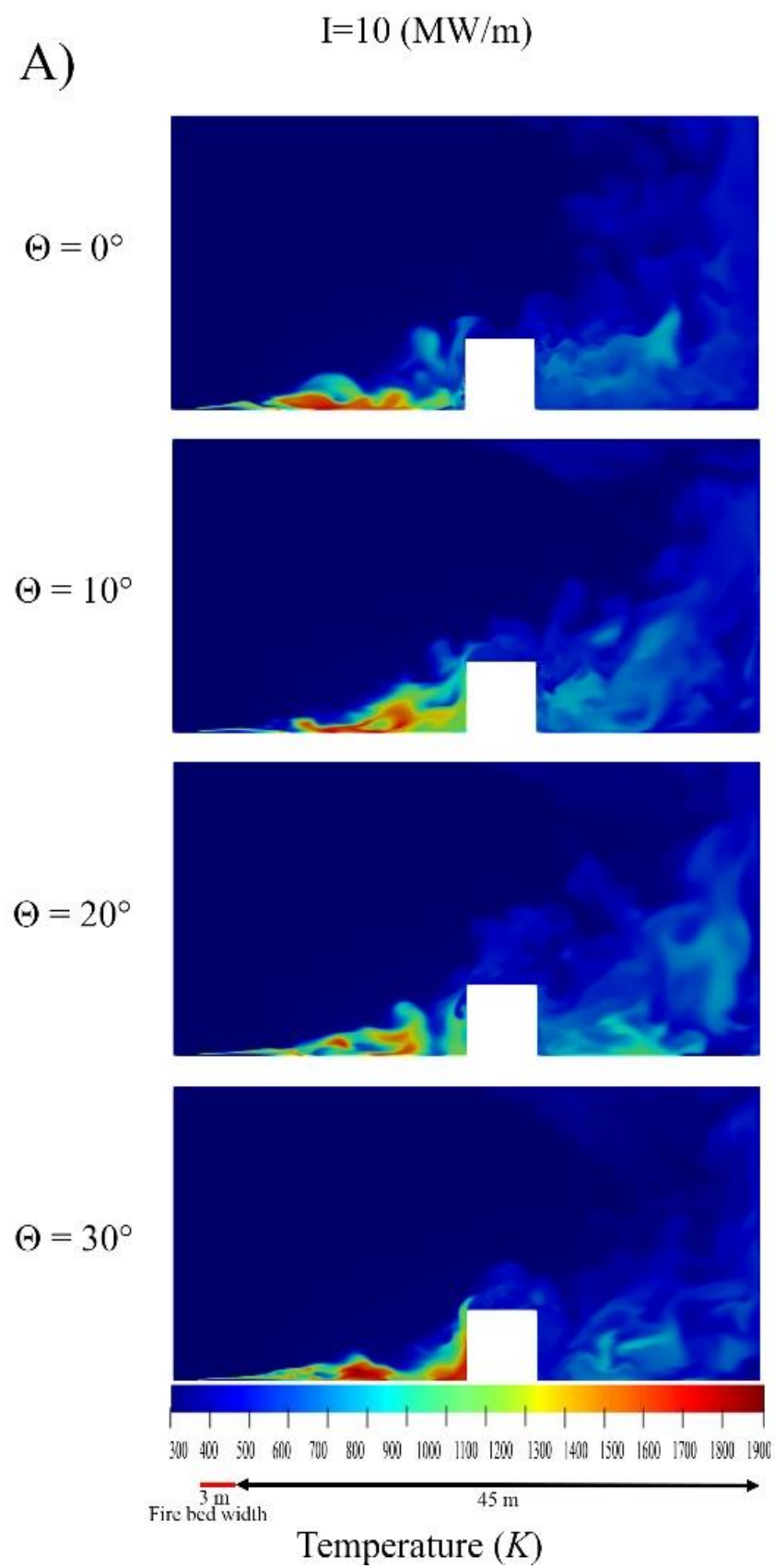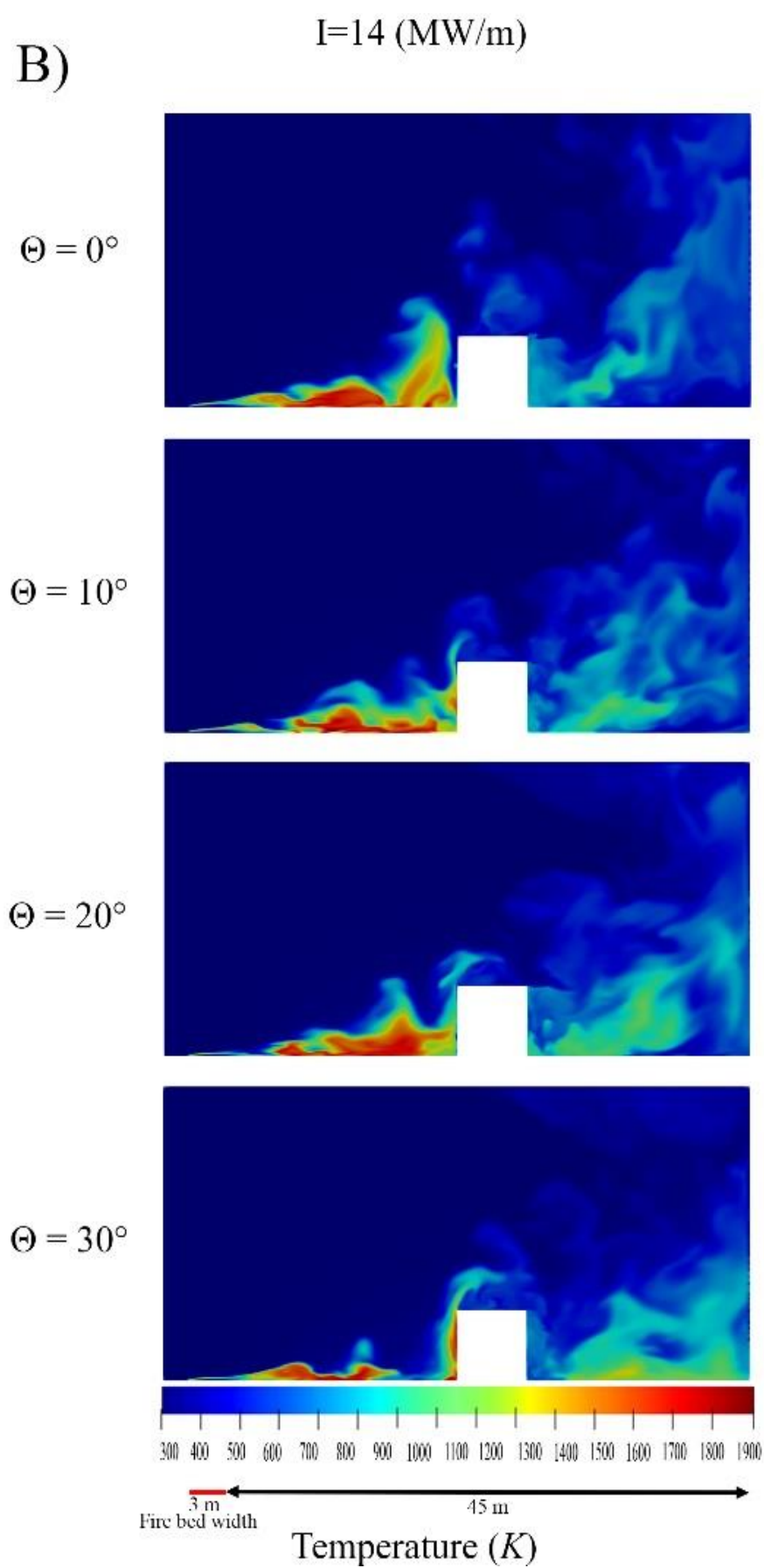
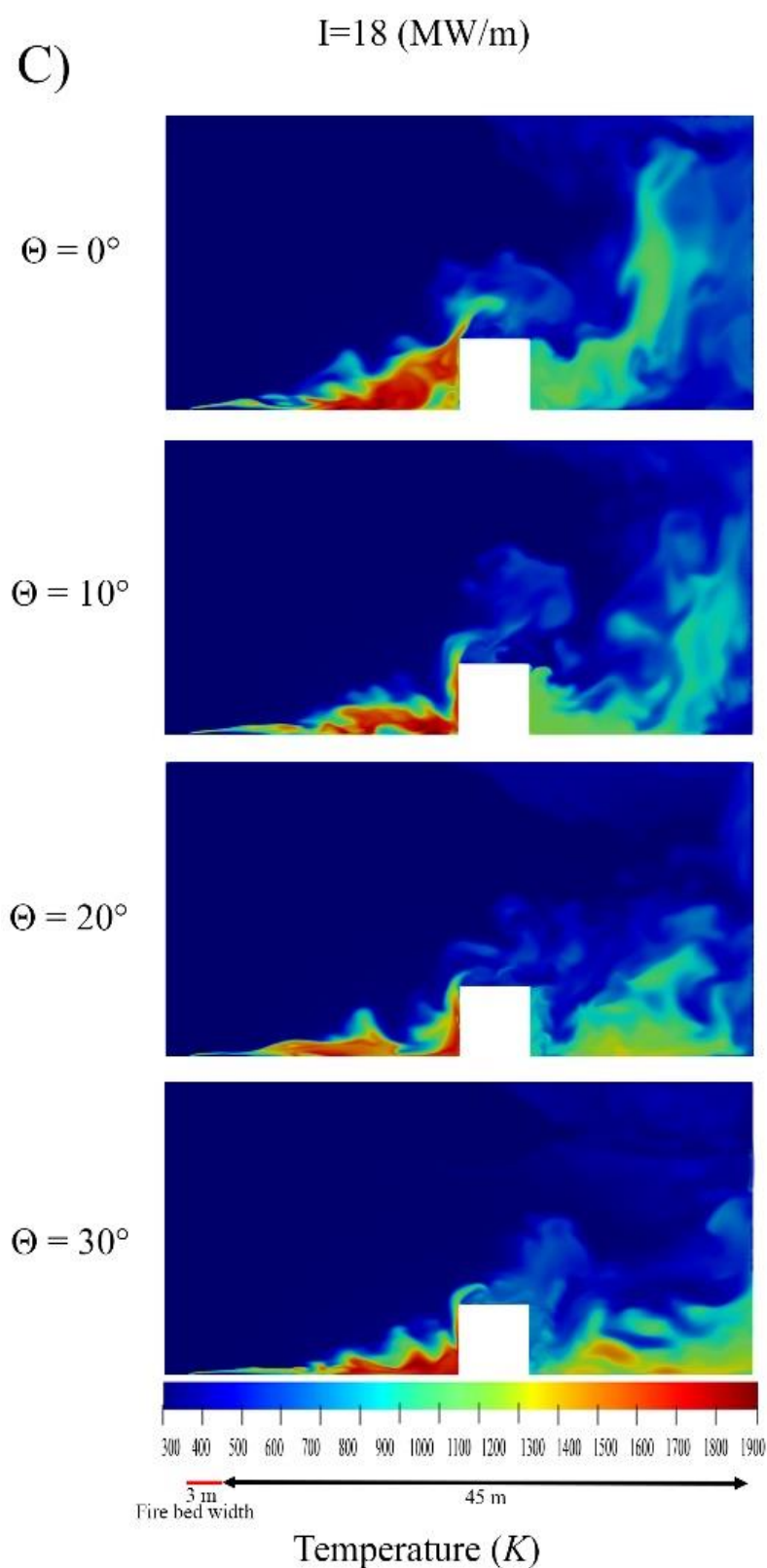**Figure 4.** *Cont.*

Figure 4. *Cont.*

Figure 4. Time-averaged plot of temperature distribution for the reference velocity U_{ref} = 6 m/s in various fire intensities and sloped terrain (**A**) Fire intensity of 10 (I = 10 MW/m), (**B**) Fire intensity of 14 (I = 14 MW/m) and (**C**) Fire intensity of 18 (I = 18 MW/m).

Looking at the contours of temperature distribution in the vicinity of the building and on the ground close to the building, it is evident that by increasing fire intensity and sloped

terrain simultaneously, areas with higher temperatures closer to the building expand. This phenomenon can be associated with the synergies of two key factors. The first is that the greater fire intensity physically implies greater fuel consumption and as a result, a higher temperature the second parameter is that by the combined growth of fire intensity and slope, the flow velocity increases which triggers an increase in the Coanda effects that trigger the flow to be more tilted to stay connected to the ground instantly downstream of the fire.

Figure 5 shows the time-averaged plots of the collective temperature of the building surface in the stabilized state of the fire, for different fire intensities and sloped terrains. The collective temperature is described as the average temperature of the entire surface including the front, back, top and side faces. The reason for defining this concept is that each point of the surface has a distinct temperature, so the collective temperature is a sensible index to capture the temperature rise on the surface of the building.
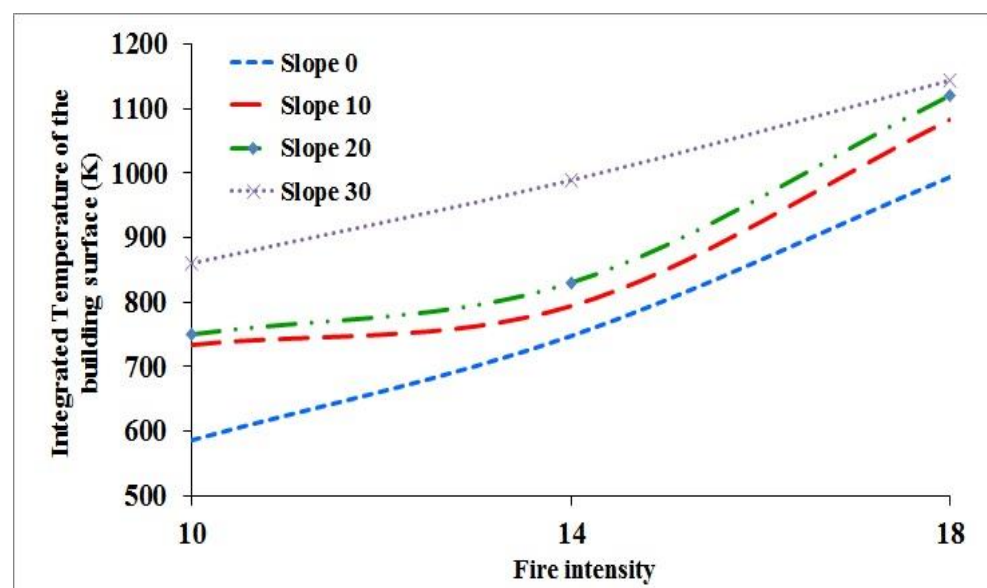

Figure 5. Integrated temperature on the building surface versus the fire intensity for a constant U_{ref} = 6 m/s and different terrain slopes.

As shown, the overall trend in this figure is matched with the results recorded in Figure 4 in that by increasing fire intensity, higher slopes experience higher mean temperature on the surface of the building. Results in Figure 5 show a sharp rise in the integrated temperature on the surface of the structure for the greater fire intensities and greater terrain slopes.

This is due to the increase in the intensity of the fire plume with the increment of the terrain slope. This is because of the growth in fire plumes, which is augmented by the wind velocity. This wind velocity is carried toward the building area that is perpendicular to the ground. Basically, the scale of fire intensity and value of terrain slope has a direct relationship with an integrated temperature of the building surface.

Demonstrated in Figure 6 is the distribution of temperature profile at the exterior of the building for various fire intensities and terrain slopes. It is evident that the surface at the front of the building experiences a more elevated temperature, which is associated with a greater view factor in terms of the radiation heat transfer received from the fire source. As can be seen from Figure 6A–C), increasing fire intensity and terrain slope would result in an upsurge in the maximum temperature on the surface of the building. The lack of stability between the buoyancy and inertial forces causes the creation of a turbulent flame which is the key reason for the random regime of the contours shown in Figure 6.
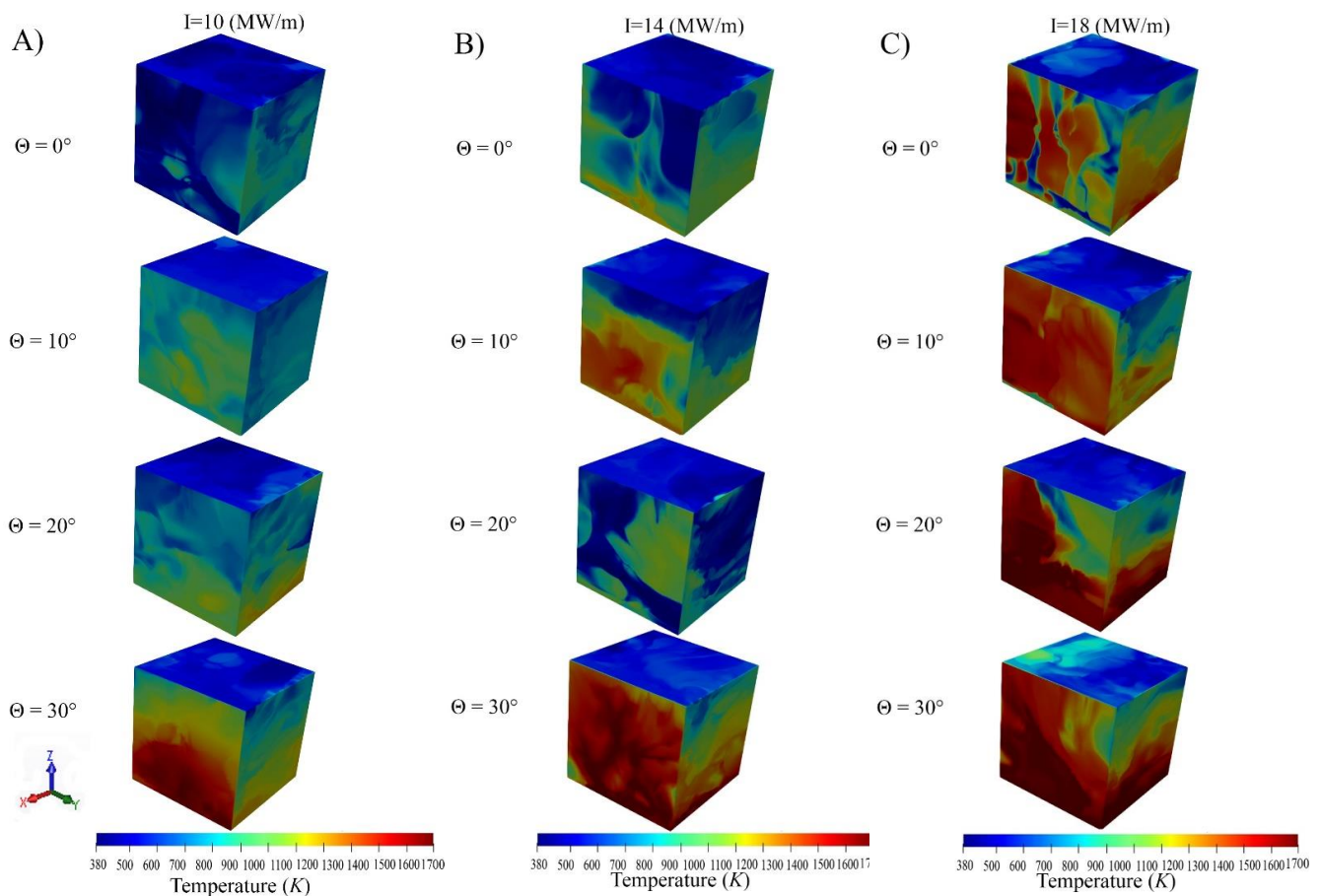
Figure 6. The time-averaged plot of the temperature distribution on the surface of the building for three different fire intensity values and terrain slope at the stabilized state of the flame (**A**) Fire intensity of 10 (I = 10 MW/m), (**B**) Fire intensity of 14 (I = 14 MW/m) and (**C**) Fire intensity of 18 (I = 18 MW/m).

Essentially, the risk of bushfire in the WUI can be explained as a joint act of fire possibility, the intensity of the fire, and fire impacts [86]. The results drawn from this research trigger some questions on the logic of risk management techniques, for instance the one in Australian Standard AS 3959 [87].

Table 1 shows the flame height for the cases with three different fire intensity values and different terrain slopes 0°, 10°, 20°, and 30°. As reported, an increase in the terrain slope, decreases the flame height, as the tilt angle increases. On the other hand, an increase in the fire intensity increases the flame height because of an increase in fuel rate consumption and flame stability.

Table 1. Comparison of the flame height for different terrain slopes and fire intensities.

	Fire Intensity 10 (MW/m)	Fire Intensity 14 (MW/m)	Fire Intensity 18 (MW/m)
Flame height (slope 0°), m	2.5	3	3.5
Flame height (slope 10°), m	2	2.8	3
Flame height (slope 20°), m	1.5	2.5	2.8
Flame height (slope 30°), m	1	1.5	2.5

Figure 7 shows the contour of dynamic pressure for the terrain with slopes 10° to 30° and various fire intensity values of 10, 14, and 18 MW/m². Comparing Figures 4 and 6,

it can be acknowledged that the pressure drops, downstream of the fire, caused by the movement of lower-dense hot air, and leads to an increase in the tilt angle of the flame.
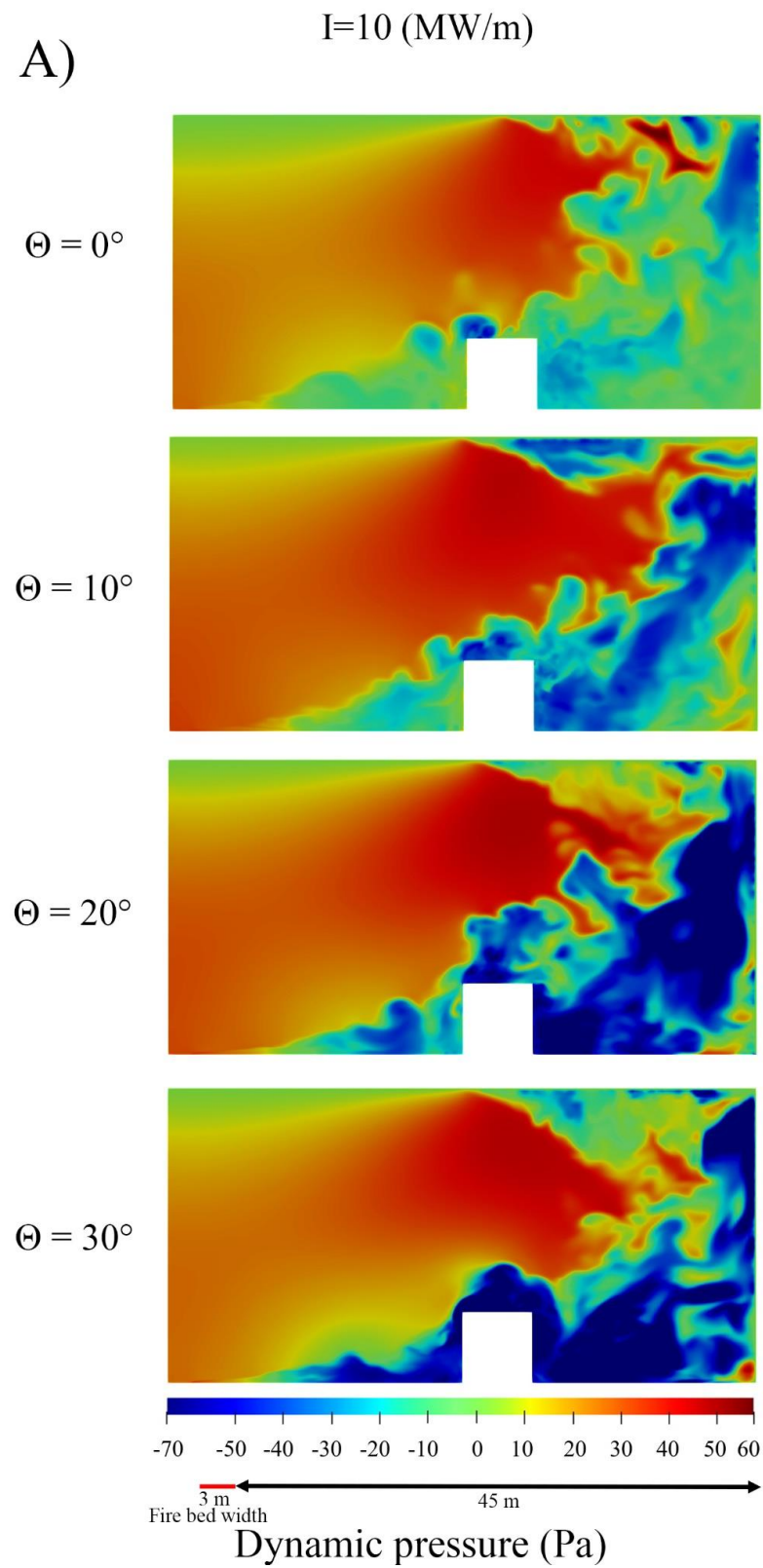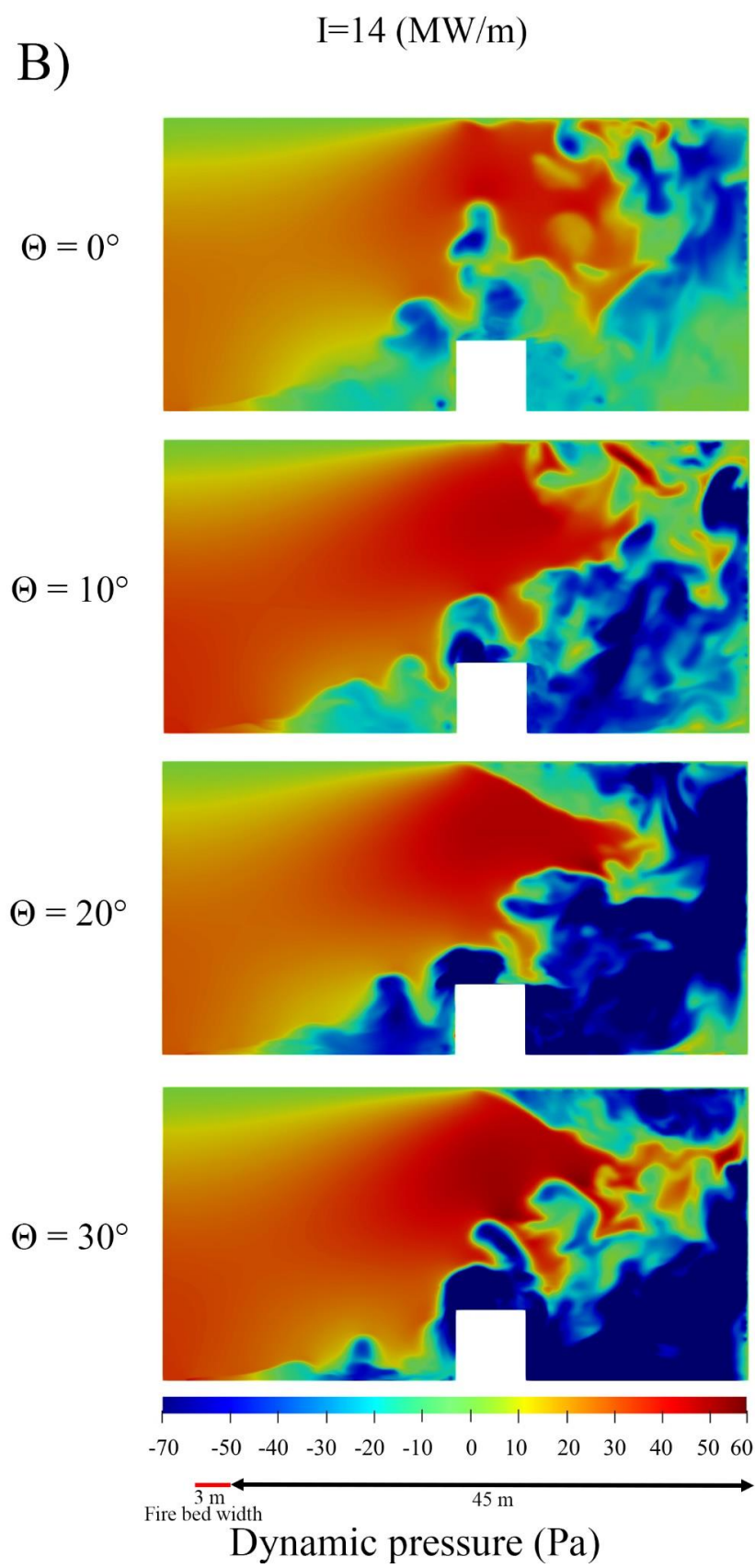

Figure 7. *Cont.*

B)

I=14 (MW/m)

$\Theta = 0°$

$\Theta = 10°$

$\Theta = 20°$

$\Theta = 30°$

-70 -50 -40 -30 -20 -10   0   10   20   30   40   50 60

3 m
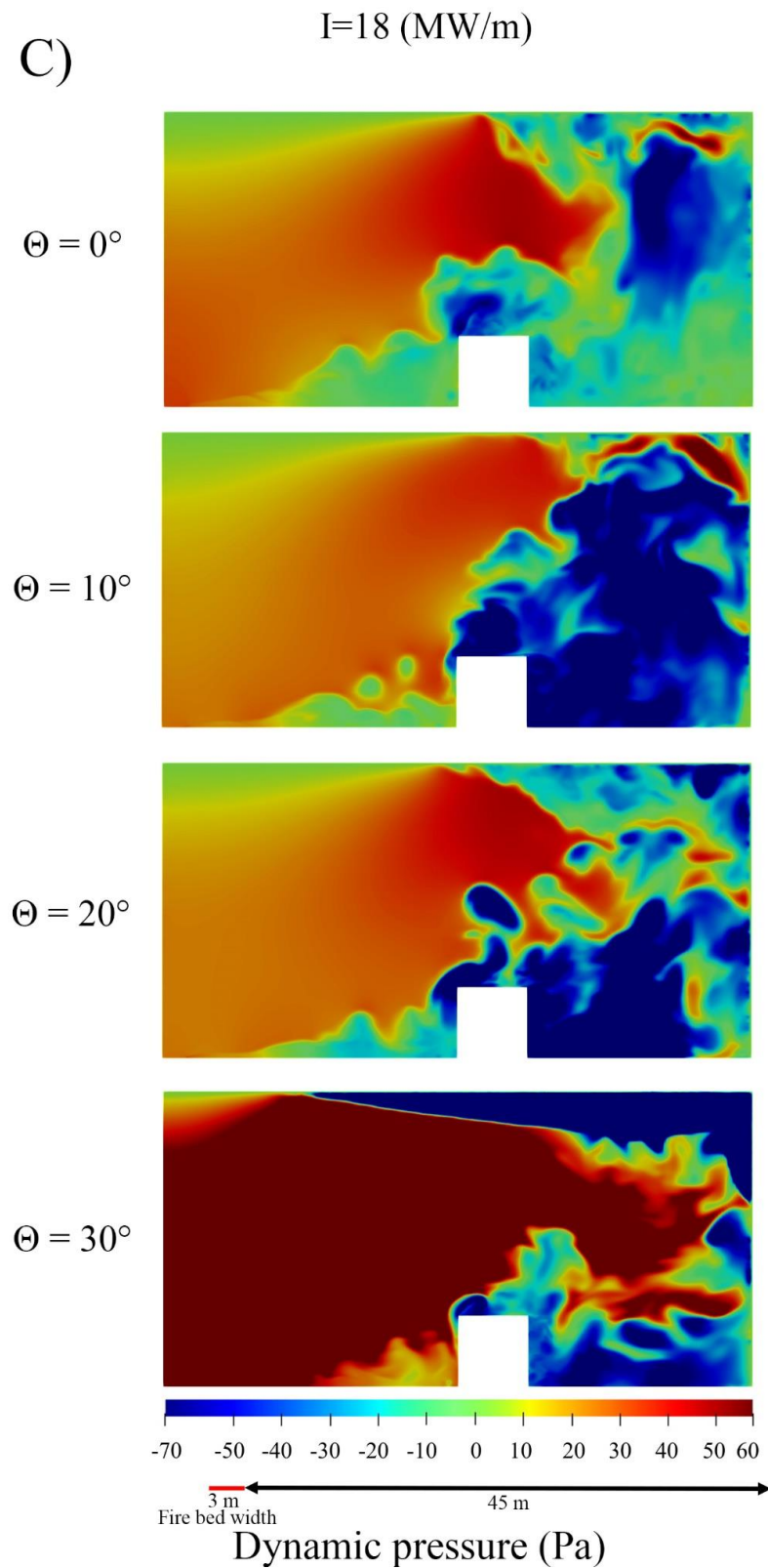Fire bed width

45 m

Dynamic pressure (Pa)

Figure 7. *Cont.*

Figure 7. Time-averaged plot of dynamic pressure for the reference velocity U_{ref} = 6 m/s in various fire intensities and sloped terrain (**A**) Fire intensity of 10 (I = 10 MW/m), (**B**) Fire intensity of 14 (I = 14 MW/m) and (**C**) Fire intensity of 18 (I = 18 MW/m).

The graph of the frequency spectrum of building surface temperature found from fast Fourier transform (FFT) analysis for the first 120 s of the simulation is shown in Figure 8.

As can be seen, an increase in the two parameters of fire intensity and terrain slope leads to frequent pulsations in the fire plume. This is due to more frequent temperature signals caused by the more movement of hot and low-dense plumes downstream of the fire bed. The dominant frequencies are for the cases with higher fire intensities and terrain slopes.
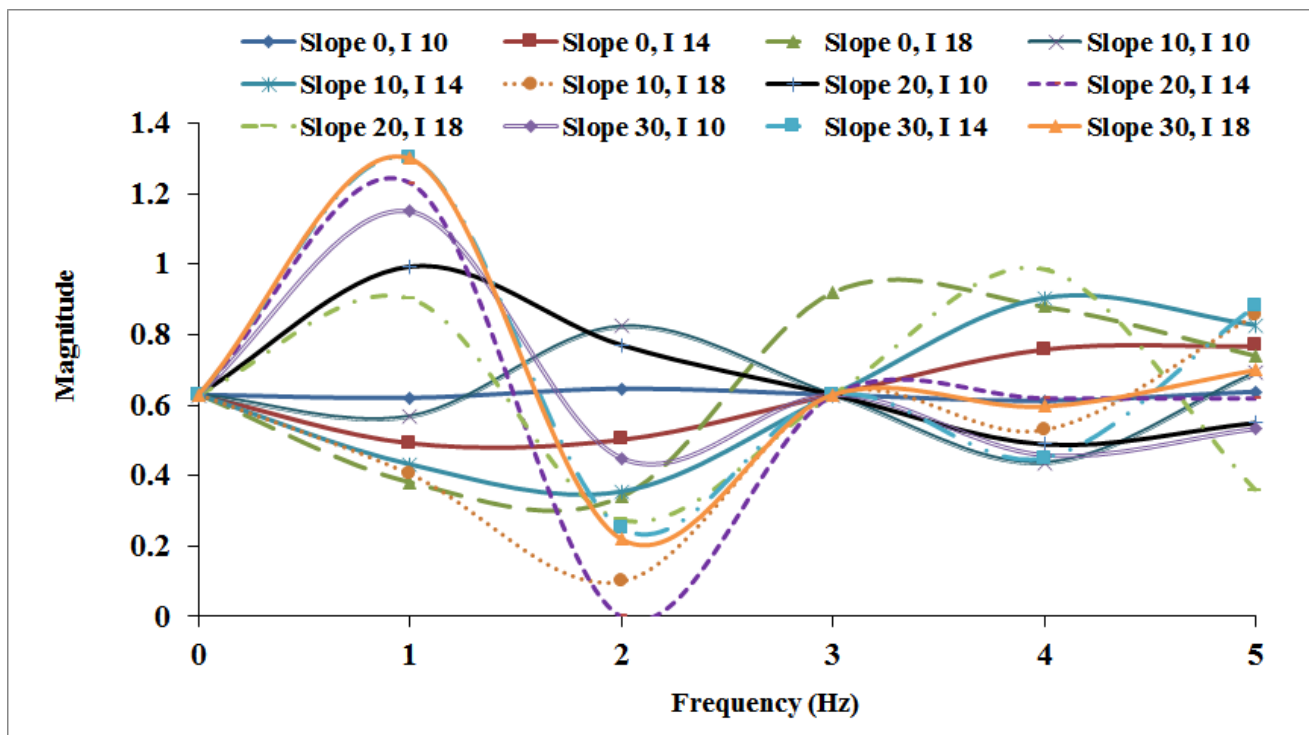

Figure 8. The graph of frequency spectrum of building surface temperature obtained from fast Fourier transform (FFT) analysis for first 120 s of the simulation for various terrain slope values and fire intensities.

6. Conclusions

A 3D CFD analysis of the dynamic characteristics of wind-driven line fires and their impacts on an idealized building has been presented, with a focus on the combined effects of fire intensity and terrain slope applicable to WUI fire impact. The model was derived from LES simulation of a wind-driven fire using a FireFOAM solver which is an open-source CFD software for fire dynamic modeling and turbulent diffusion flames. The numerical findings were compared with the empirical findings in no fire condition and demonstrated to be aligned with the experimental data.

A detailed comparison of the dynamics of the fire's plume with a series of fire intensities on the structure located on different upslope terrains revealed that the collective effect of fire intensity and terrain slope changes the plume geometry and characteristics, also the presence of a building can considerably change the plume attachment pattern. Concurrent raise in fire intensity and terrain slope causes a significant increase of the temperature downstream of the source of fire in such a way that even at the back of the building a zone of a particularly higher temperature can be seen. It should be noted that by enhancing the terrain slope from $10°$ to $30°$ in the constant fire intensity of 10 MW/m^2, the integrated temperature of the building increases approximately 46%. In addition, rising the intensity of the fire from 10 to 18 MW/m^2 increases the building temperature by approximately 55%.

In addition, the presence of a building can substantially contributes to changing the plume attachment length. In other words, with increasing fire intensity and terrain slope the building generates premature buoyant instabilities and the fire plume lift-off distance lessens in front of the building.

It was also noticed that the presence of the building enhances the plume's irregularity and regional heat transfer at certain positions upstream of the building. Therefore, possible dangerous areas vulnerable to the new fire source generation can be formed close to the building. In addition, the ability of the current model to estimate the thermal response of the building to the fire with increasing fire intensity on hilly terrain (upslope) was studied. It was noted the flame front was progressively tilted ahead as the slope increased from $\theta = 10°$ to $\theta = 30°$, and also a concurrent increase in fire intensity and terrain slope will enhance this tilt angle and made it more connected to the ground.

The increased tilt angle of the fire's plume with up-sloped terrain is mainly due to the Coanda effect which demands the plume to be tilted to the floor instantly downstream of the fire bed. The Coanda effects turn out to be stronger in greater upslope angles, as in these situations, besides the wind force, a buoyancy force is also generated windward which reinforces the Coanda effects and creates more inclination and makes the fire plume more connected to the ground.

Using the results offered in the present study at different scales, some knowledge will be gained on specific susceptibilities and the usefulness of mitigation strategies in WUI communities. Although it needs a high computational expense to fully apply the suggested context at greater scales, this attempt could suggest a somewhat reliable solution to lessen risks from potential WUI fires. These outcomes can be expanded by performing comparable analyses with fires having a range of characteristics, and more realistic and practical building geometries or multiple structures. In addition, more research is necessary to investigate fire dynamic behavior and to estimate more locally, justifiable space around homes. There is a big gap in fire science research to find feasible strategies for fire exposure mitigation from both radiation and direct flame contact. Such studies are essential to advise thorough wildfire risk management plans, together with enhanced urban development, and WUI building design.

Author Contributions: Conceptualization, M.G. and A.S.; methodology, M.G.; software, M.G. and A.E.-N.; validation, M.G.; formal analysis, M.G.; investigation, M.G.; resources, M.G.; data curation, M.G. and A.E.-N.; writing—original draft preparation, M.G.; writing—review and editing, A.S. and M.G.; visualization, M.G.; supervision, A.S. and M.G.; project administration, A.E.-N. All authors have read and agreed to the published version of the manuscript.

Institutional Review Board Statement: Not applicable.

Informed Consent Statement: Not applicable.

Data Availability Statement: The data presented in this study are available on request from the corresponding author.

Conflicts of Interest: The authors declare no conflict of interest.

Abbreviations

c_p	heat capacity (J/kg/K)
f	frequency (Hz)
g	gravitational acceleration (m/s^2)
h_s	sensible enthalpy (J/kg)
j	mass diffusive flux (kg/m^2/s)
N_s	number of species
p	pressure (Pa)
Pr	Prandtl number
$\dot{q}_c'''$	heat release per unit volume (W/m^3)
$\dot{q}_r''$	radiative flux (W/m^2)

Q	Q-criterion
Sc	Schmidt number
t	time (s)
T	temperature (K)
U/u	velocity (m/s)
Greek	
α	thermal diffusivity (kg/m/s)
μ	dynamic viscosity (kg/m/s)
ρ	density (kg/m^3)
$\dot{\omega}_k'''$	reaction rate (kg/m^3/s)
Subscripts	
c	combustion
i, j, k	coordinate index
k	specie *mix* mixture
r	radiative
sgs	sub-grid scale
t	turbulent
ref	reference value
Superscripts	
T	transpose

References

1. Sullivan, A.L. Wildland surface fire spread modelling, 1990–2007. 2: Empirical and quasi-empirical models. *Int. J. Wildland Fire* **2009**, *18*, 369–386. [CrossRef]
2. Finney, M.A. The challenge of quantitative risk analysis for wildland fire. *For. Ecol. Manag.* **2005**, *211*, 97–108. [CrossRef]
3. Sharples, J.J.; McRae, R.H.; Wilkes, S.R. Wind–terrain effects on the propagation of wildfires in rugged terrain: Fire channelling. *Int. J. Wildland Fire* **2012**, *21*, 282–296. [CrossRef]
4. McArthur, A.G. *Weather and Grassland Fire Behavior*; Department of National Development, Forestry and Timber Bureau: Canberra, Australia, 1966; Volume 107, p. 23.
5. Rothermel, R.C. A mathematical model for predicting fire spread in wildland fuels. In *Intermountain Forest & Range Experiment Station, Forest Service*; US Department of Agriculture: Logan, UT, USA, 1972.
6. Noble, I.R.; Gill, A.M.; Bary, G.A. McArthur's fire-danger meters expressed as equations. *Aust. J. Ecol.* **1980**, *5*, 201–203. [CrossRef]
7. Sharples, J.J. Review of formal methodologies for wind–slope correction of wildfire rate of spread. *Int. J. Wildland Fire* **2008**, *17*, 179–193. [CrossRef]
8. Dupuy, J.L.; Maréchal, J. Slope effect on laboratory fire spread: Contribution of radiation and convection to fuel bed preheating. *Int. J. Wildland Fire* **2011**, *20*, 289–307. [CrossRef]
9. Van Wagner, C.E. *Fire Behaviour Mechanisms in a Red Pine Plantation*; Canadian Forest Service: Victoria, BC, Canada, 1968.
10. Viegas, D.X. Fire line rotation as a mechanism for fire spread on a uniform slope. *Int. J. Wildland Fire* **2002**, *11*, 11–23. [CrossRef]
11. Dupuy, J.L. Slope and fuel load effects on fire behavior: Laboratory experiments in pine needles fuel beds. *Int. J. Wildland Fire* **1995**, *5*, 153–164. [CrossRef]
12. Weise, D.R.; Biging, G.S. A qualitative comparison of fire spread models incorporating wind and slope effects. *For. Sci.* **1997**, *43*, 170–180.
13. Mendes-Lopes, J.M.; Ventura, J.M.; Amaral, J.M. Flame characteristics, temperature–time curves, and rate of spread in fires propagating in a bed of Pinus pinaster needles. *Int. J. Wildland Fire* **2003**, *12*, 67–84. [CrossRef]
14. Vega, J.A.; Cuiñas, P.; Fonturbel, T.; Pérez-Gorostiaga, P.; Fernandez, C. Predicting fire behaviour in Galician (NW Spain) shrubland fuel complexes. In Proceedings of the 3rd International Conference on Forest Fire Research and 14th Conference on Fire and Forest Meteorology, Coimbra, Portugal, 16 November 1998; Volume 2, pp. 16–20.
15. Fernandes, P.M.; Botelho, H.S.; Rego, F.C.; Loureiro, C. Empirical modelling of surface fire behaviour in maritime pine stands. *Int. J. Wildland Fire* **2009**, *18*, 698–710. [CrossRef]
16. Cheney, N.P.; Gould, J.S.; Catchpole, W.R. The influence of fuel, weather and fire shape variables on fire-spread in grasslands. *Int. J. Wildland Fire* **1993**, *3*, 31–44. [CrossRef]
17. Dupuy, J.L.; Maréchal, J.; Portier, D.; Valette, J.C. The effects of slope and fuel bed width on laboratory fire behaviour. *Int. J. Wildland Fire* **2011**, *20*, 272–288. [CrossRef]
18. Edalati-nejad, A.; Ghodrat, M.; Simeoni, A. Numerical investigation of the effect of sloped terrain on wind-driven surface fire and its impact on idealized structures. *Fire* **2021**, *4*, 94. [CrossRef]
19. Eftekharian, E.; Rashidi, M.; Ghodrat, M.; He, Y.; Kwok, K.C. LES simulation of terrain slope effects on wind enhancement by a point source fire. *Case Stud. Therm. Eng.* **2020**, *18*, 100588. [CrossRef]
20. Malanson, G.P. Intensity as a third factor of disturbance regime and its effect on species diversity. *Oikos* **1984**, *43*, 411–413. [CrossRef]

21. Edalati-nejad, A.; Ghodrat, M.; Fanaee, S.A.; Simeoni, A. Numerical Simulation of the Effect of Fire Intensity on Wind Driven Surface Fire and Its Impact on an Idealized Building. *Fire* **2022**, *5*, 17. [CrossRef]

22. Keeley, J.E.; McGinnis, T.W. Impact of prescribed fire and other factors on cheatgrass persistence in a Sierra Nevada ponderosa pine forest. *Int. J. Wildland Fire* **2007**, *16*, 96–106. [CrossRef]

23. Keeley, J.E. Fire intensity, fire severity and burn severity: A brief review and suggested usage. *Int. J. Wildland Fire* **2009**, *18*, 116–126. [CrossRef]

24. Byram, G.M. Combustion of forest fuels. *For. Fire Control Use* **1959**, 61–89. Available online: https://www.scirp.org/(S(351jmbntvnsjt1aadkposzje))/reference/ReferencesPapers.aspx?ReferenceID=1938996 (accessed on 23 October 2022).

25. Hirsch, K.G.; Martell, D.L. A review of initial attack fire crew productivity and effectiveness. *Int. J. Wildland Fire* **1996**, *6*, 199–215. [CrossRef]

26. Finney, M.A.; Cohen, J.D.; McAllister, S.S.; Jolly, W.M. On the need for a theory of wildland fire spread. *Int. J. Wildland Fire* **2012**, *22*, 25–36. [CrossRef]

27. Sullivan, A.L. A review of wildland fire spread modelling, 1990-present, 1: Physical and quasi-physical models. *arXiv* **2007**, arXiv:0706.3074.

28. Michaletz, S.T.; Johnson, E.A. Fire and biological processes. *J. Veg. Sci.* **2003**, *14*, 622–623. [CrossRef]

29. Chatto, K.; Tolhurst, K.G. A review of the relationship between fireline intensity and the ecological and economic effects of fire, and methods currently used to collect fire data. In *Department of Sustainability and Environment*; Forest Science Centre: Heidelberg, Australia, 2004.

30. Williams, R.J.; Cook, G.D.; Gill, A.M.; Moore, P.H. Fire regime, fire intensity and tree survival in a tropical savanna in northern Australia. *Aust. J. Ecol.* **1999**, *24*, 50–59. [CrossRef]

31. Auld Td O'connell, M.a. Predicting patterns of post-fire germination in 35 eastern Australian Fabaceae. *Aust. J. Ecol.* **1991**, *16*, 53–70. [CrossRef]

32. O'Connor, C.; Miller, R.; Bates, J.D. Vegetation response to western juniper slash treatments. *Environ. Manag.* **2013**, *52*, 553–566. [CrossRef]

33. Bradstock, R.A.; Auld, T.D. Soil temperatures during experimental bushfires in relation to fire intensity: Consequences for legume germination and fire management in south-eastern Australia. *J. Appl. Ecol.* **1995**, 76–84. [CrossRef]

34. Brooks, M.L. Peak fire temperatures and effects on annual plants in the Mojave Desert. *Ecol. Appl.* **2002**, *12*, 1088–1102. [CrossRef]

35. Keeley, J.E.; Baer-Keeley, M.; Fotheringham, C.J. Alien plant dynamics following fire in Mediterranean-climate California shrublands. *Ecol. Appl.* **2005**, *15*, 2109–2125. [CrossRef]

36. Wooster, M.J.; Zhukov, B.; Oertel, D. Fire radiative energy for quantitative study of biomass burning: Derivation from the BIRD experimental satellite and comparison to MODIS fire products. *Remote Sens. Environ.* **2003**, *86*, 83–107. [CrossRef]

37. Dennison, P.E. Fire detection in imaging spectrometer data using atmospheric carbon dioxide absorption. *Int. J. Remote Sens.* **2006**, *27*, 3049–3055. [CrossRef]

38. Caton, S.E.; Hakes, R.S.; Gorham, D.J.; Zhou, A.; Gollner, M.J. Review of pathways for building fire spread in the wildland urban interface part I: Exposure conditions. *Fire Technol.* **2017**, *53*, 429–473. [CrossRef]

39. Hakes, R.S.; Caton, S.E.; Gorham, D.J.; Gollner, M.J. A review of pathways for building fire spread in the wildland urban interface part II: Response of components and systems and mitigation strategies in the United States. *Fire Technol.* **2017**, *53*, 475–515. [CrossRef]

40. Sharples, J.J.; McRae, R.H.; Weber, R.O. Wind characteristics over complex terrain with implications for bushfire risk management. *Environ. Model. Softw.* **2010**, *25*, 1099–1120. [CrossRef]

41. Dahale, A.; Ferguson, S.; Shotorban, B.; Mahalingam, S. Effects of distribution of bulk density and moisture content on shrub fires. *Int. J. Wildland Fire* **2013**, *22*, 625–641. [CrossRef]

42. Pimont, F.; Dupuy, J.L.; Linn, R.R.; Dupont, S. Impacts of tree canopy structure on wind flows and fire propagation simulated with FIRETEC. *Ann. For. Sci.* **2011**, *68*, 523–530. [CrossRef]

43. Linn, R.R.; Canfield, J.M.; Cunningham, P.; Edminster, C.; Dupuy, J.L.; Pimont, F. Using periodic line fires to gain a new perspective on multi-dimensional aspects of forward fire spread. *Agric. For. Meteorol.* **2012**, *157*, 60–76. [CrossRef]

44. Frangieh, N.; Accary, G.; Morvan, D.; Meradji, S.; Bessonov, O. Wildfires front dynamics: 3D structures and intensity at small and large scales. *Combust. Flame* **2020**, *211*, 54–67. [CrossRef]

45. Mueller, E.V.; Gallagher, M.R.; Skowronski, N.; Hadden, R.M. Approaches to Modeling Bed Drag in Pine Forest Litter for Wildland Fire Applications. *Transp. Porous Media* **2021**, *138*, 637–660. [CrossRef]

46. McGrattan, K.; Hostikka, S.; McDermott, R.; Floyd, J.; Weinschenk, C.; Overholt, K. Fire dynamics simulator user's guide. *NIST Spec. Publ.* **2013**, *1019*, 1–339.

47. Mueller, E.V.; Campbell-Lochrie, Z.; Mell, W.; Hadden, R.M. Numerical Simulation of Low-Intensity Fire Spread in Pine Litter. 2018. Available online: http://hdl.handle.net/10316.2/44517 (accessed on 12 January 2021).

48. Mell, W.; Maranghides, A.; McDermott, R.; Manzello, S.L. Numerical simulation and experiments of burning douglas fir trees. *Combust. Flame* **2009**, *156*, 2023–2041. [CrossRef]

49. Mueller, E.; Mell, W.; Simeoni, A. Large eddy simulation of forest canopy flow for wildland fire modeling. *Can. J. For. Res.* **2014**, *44*, 1534–1544. [CrossRef]

50. Poletto, R.; Craft, T.; Revell, A. A new divergence free synthetic eddy method for the reproduction of inlet flow conditions for LES. *Flow Turbul. Combust.* **2013**, *91*, 519–539. [CrossRef]

51. Hostikka, S.I.; Mangs, J.O.; Mikkola, E.S. Comparison of two and three dimensional simulations of fires at wildland urban interface. *Fire Saf. Sci.* **2009**, *9*, 1353–1364. [CrossRef]

52. Linn, R.R.; Winterkamp, J.L.; Weise, D.R.; Edminster, C. A numerical study of slope and fuel structure effects on coupled wildfire behaviour. *Int. J. Wildland Fire* **2010**, *19*, 179–201. [CrossRef]

53. Mell, W.E.; Manzello, S.L.; Maranghides, A.; Butry, D.; Rehm, R.G. The wildland–urban interface fire problem–current approaches and research needs. *Int. J. Wildland Fire* **2010**, *19*, 238–251. [CrossRef]

54. Morvan, D. Physical phenomena and length scales governing the behaviour of wildfires: A case for physical modelling. *Fire Technol.* **2011**, *47*, 437–460. [CrossRef]

55. Miller, C.; Urban, D.L. Connectivity of forest fuels and surface fire regimes. *Landsc. Ecol.* **2000**, *15*, 145–154. [CrossRef]

56. Moinuddin, K.; Khan, N.; Sutherland, D. Numerical study on effect of relative humidity (and fuel moisture) on modes of grassfire propagation. *Fire Saf. J.* **2021**, *125*, 103422. [CrossRef]

57. Miller, C.; Urban, D.L. A model of surface fire, climate and forest pattern in the Sierra Nevada, California. *Ecol. Model.* **1999**, *114*, 113–135. [CrossRef]

58. Morandini, F.; Silvani, X.; Dupuy, J.L.; Susset, A. Fire spread across a sloping fuel bed: Flame dynamics and heat transfers. *Combust. Flame* **2018**, *190*, 158–170. [CrossRef]

59. García-Llamas, P.; Suárez-Seoane, S.; Fernández-Manso, A.; Quintano, C.; Calvo, L. Evaluation of fire severity in fire prone-ecosystems of Spain under two different environmental conditions. *J. Environ. Manag.* **2020**, *271*, 110706. [CrossRef]

60. Hilton, J.; Garg, N. Rapid wind–terrain correction for wildfire simulations. *Int. J. Wildland Fire* **2021**, *30*, 410–427. [CrossRef]

61. Sullivan, A.L.; Sharples, J.J.; Matthews, S.; Plucinski, M.P. A downslope fire spread correction factor based on landscape-scale fire behaviour. *Environ. Model. Softw.* **2014**, *62*, 153–163. [CrossRef]

62. Clements, C.B.; Seto, D. Observations of fire–atmosphere interactions and near-surface heat transport on a slope. *Bound.-Layer Meteorol.* **2015**, *154*, 409–426. [CrossRef]

63. Sharples, J.J. An overview of mountain meteorological effects relevant to fire behaviour and bushfire risk. *Int. J. Wildland Fire* **2009**, *18*, 737–754. [CrossRef]

64. Simpson, C.C.; Sharples, J.J.; Evans, J.P. Sensitivity of atypical lateral fire spread to wind and slope. *Geophys. Res. Lett.* **2016**, *43*, 1744–1751. [CrossRef]

65. Wang, Y.; Chatterjee, P.; de Ris, J.L. Large eddy simulation of fire plumes. *Proc. Combust. Inst.* **2011**, *33*, 2473–2480. [CrossRef]

66. Ghaderi, M.; Ghodrat, M.; Sharples, J.J. LES Simulation of Wind-Driven Wildfire Interaction with Idealized Structures in the Wildland-Urban Interface. *Atmosphere* **2021**, *12*, 21. [CrossRef]

67. Richards, P.J.; Hoxey, R.P. Pressures on a cubic building—Part 1: Full-scale results. *J. Wind. Eng. Ind. Aerodyn.* **2012**, *102*, 72–86. [CrossRef]

68. Richards, P.; Norris, S. LES modelling of unsteady flow around the Silsoe cube. *J. Wind. Eng. Ind. Aerodyn.* **2015**, *144*, 70–78. [CrossRef]

69. Smith, S.T. The Performance of Distribution Utility Poles in Wildland Fire Hazard Areas. *Tech. Bull* **2014**.

70. Wu, X. Inflow turbulence generation methods. *Annu. Rev. Fluid Mech.* **2017**, *49*, 23–49. [CrossRef]

71. Tominaga, Y.; Mochida, A.; Yoshie, R.; Kataoka, H.; Nozu, T.; Yoshikawa, M.; Shirasawa, T. AIJ guidelines for practical applications of CFD to pedestrian wind environment around buildings. *J. Wind. Eng. Ind. Aerodyn.* **2008**, *96*, 1749–1761. [CrossRef]

72. Greenshields, C.J. *OpenFOAM User Guide*; OpenFOAM Foundation Ltd.: London, UK, 2015; p. 473.

73. Liu, H.; Wang, C.; Zhang, A. Numerical simulation of the wood pyrolysis with homogenous/heterogeneous moisture using FireFOAM. *Energy* **2020**, *201*, 117624. [CrossRef]

74. Myers, T.; Trouvé, A.; Marshall, A. Predicting sprinkler spray dispersion in FireFOAM. *Fire Saf. J.* **2018**, *100*, 93–102. [CrossRef]

75. Ren, N.; Wang, Y.; Vilfayeau, S.; Trouvé, A. Large eddy simulation of turbulent vertical wall fires supplied with gaseous fuel through porous burners. *Combust. Flame* **2016**, *169*, 194–208. [CrossRef]

76. El Houssami, M.; Lamorlette, A.; Morvan, D.; Hadden, R.M.; Simeoni, A. Framework for submodel improvement in wildfire modeling. *Combust. Flame* **2018**, *190*, 12–24. [CrossRef]

77. Favre, A. Turbulence: Space-time statistical properties and behavior in supersonic flows. *Phys. Fluids* **1983**, *26*, 2851–2863. [CrossRef]

78. Magnussen, B.F.; Hjertager, B.H. On mathematical modeling of turbulent combustion with special emphasis on soot formation and combustion. In *Symposium (International) on Combustion*; Elsevier: Amsterdam, The Netherlands, 1977; Volume 16, pp. 719–729.

79. Magnussen, B.F.; Hjertager, B.H.; Olsen, J.G.; Bhaduri, D. Effects of turbulent structure and local concentrations on soot formation and combustion in C2H2 diffusion flames. In *Symposium (International) on Combustion*; Elsevier: Amsterdam, The Netherlands, 1979; Volume 17, pp. 1383–1393.

80. Wang, C.J.; Wen, J.X.; Chen, Z.B.; Dembele, S. Predicting radiative characteristics of hydrogen and hydrogen/methane jet fires using FireFOAM. *Int. J. Hydrog. Energy* **2014**, *39*, 20560–20569. [CrossRef]

81. Almeida, Y.P.; Lage, P.L.; Silva, L.F. Large eddy simulation of a turbulent diffusion flame including thermal radiation heat transfer. *Appl. Therm. Eng.* **2015**, *81*, 412–425. [CrossRef]

82. Castro, I.P.; Robins, A.G. The flow around a surface-mounted cube in uniform and turbulent streams. *J. Fluid Mech.* **1977**, *79*, 307–335. [CrossRef]

83. He, Y.; Kwok, K.; Douglas, G.; Razali, I. Numerical investigation of bushfire-wind interaction and its impact on building structure. *Fire Saf. Sci.* **2011**, *10*, 1449–1462. [CrossRef]

84. Gallacher, J.R.; Ripa, B.; Butler, B.W.; Fletcher, T.H. Lab-scale observations of flame attachment on slopes with implications for firefighter safety zones. *Fire Saf. J.* **2018**, *96*, 93–104. [CrossRef]

85. Verma, M.K. *Physics of Buoyant Flows: From Instabilities to Turbulence*; World Scientific: Singapore, 2018.

86. Mitsopoulos, I.; Mallinis, G.; Arianoutsou, M. Wildfire risk assessment in a typical Mediterranean wildland–urban interface of Greece. *Environ. Manag.* **2015**, *55*, 900–915. [CrossRef]

87. Debnam, G.; Chow, V.; England, P. *AS 3959 Construction of Buildings In Bushfire-Prone Areas–Draft For Public Comment (Dr 05060) Review of Calculation Methods And Assumptions*; Environmental Science: Sydney, Australia, 2005.